46th AIAA Aerospace Sciences Meeting and Exhibit
7 - 10 January 2008, Reno, Nevada

AIAA 2008-758

Development of An Adaptive Space-Time Method for High-Order Resolution of Discontinuities

Zhi Yang *, Dimitri J. Mavriplis †

Department of Mechanical Engineering, University of Wyoming, Laramie, WY 82071

An adaptive implicit high-order space-time method is developed for the efficient solution of time dependent partial differential equations. Time and space are treated in the same way so that the conservation laws are satisfied in both time and space coordinates, even when the mesh is moved. The adaptive strategy is mesh motion/r-refinement. To enable high order accuracy for discontinuous solutions in the absence of a limiter, the discontinuity is tracked by the ghost fluid method and then fitted by r-refinement. The efficiency and accuracy of this method are illustrated on solutions of the one-dimensional wave equation and Burger's equation.

I. Introduction

Recent advances in computational hardware capabilities have been accompanied with a desire to radically increase simulation accuracy in both space and time. Many highly accurate numerical methods have been developed in recent years. These methods include the Discontinuous Galerkin(DG) method,[5,9] the Spectral difference (SD) method[22] and the spectral volume (SV) method.[36,37] However, all high-order methods produce numerical oscillations at discontinuities due to the errors caused by using a continuous function in approximating the discontinuity, such as shocks. This is the so-called Gibbs phenomena. Researchers have developed many techniques to treat discontinuities numerically, such as shock fitting, shock capturing by limiting,[28] artificial viscosity methods,[27] and shock tracking.[1,33] In 1983, Harten[16] found that by adjusting the grid, shocks could be captured sharply without any oscillations. In later work, Yoseph[4] used aligned elements to achieve sharp shock capturing, and Trepanier[34] developed a dynamic discontinuity tracking method to achieve shock fitting. These methods rely on tracking the discontinuity: moving the grid points to the discontinuity and solving a Riemann problem at the discontinuity. These methods can also be viewed as an adaptive meshing approach, often referred to as r-refinement. Mavriplis[24] showed that high-order spectral element methods could achieve better efficiency when combined with adaptive methods, and that sharp gradients and singularities can be resolved optimally. Adaptive meshing methods may be classified as: r-refinement, h-refinement and p-refinement,[10,15,29] where r-refinement[17] refers to mesh motion or deformation, h-refinement refers to the subdivision of elements and p-refinement refers to adjusting the polynomial degree. Houston[18] has reviewed the hp-adaptive method and claims that the key to designing an adaptive scheme is to use hp-refinement in such a way that maximum reduction in the error per unit cost is achieved. Usually, if the solution is smooth or locally smooth, p-refinement may achieve better efficiency for reducing the error per unit cost. Therefore, r-refinement and h-refinement should be employed on the elements where the discontinuities occur, while p-refinement exploits more accuracy on the elements in the neighborhood of a smooth solution. Yamaleev and Carpenter[38] investigated h-refinement for the supersonic steady flow around a cylinder. Their numerical solutions showed that adding grid points near the shock improved the numerical solution accuracy only on very fine grids, and the grid adaptation did not reduce error in the pressure integral across the shock compared to that on the uniform grid. Therefore, careful consideration of adaptive meshing techniques is required to consistently improve solution accuracy at low computational cost in the presence of discontinuities. In this paper, we focus on r-refinement techniques. If grid points can be moved to the position of discontinuities in the computational domain, then the shocks only exist on

*Postdoctoral research associate, AIAA member; email: zyang@uwyo.edu
†Professor, AIAA Associate Fellow; email: mavriplis@uwyo.edu

the interfaces of the elements. The solution in each element will be smooth and *hp*-refinement will provide optimal accuracy. For unsteady flow simulations, both temporal and spatial accuracy must be considered simultaneously, and computational expense remains an important issue. Many researchers have investigated and compared higher-order implicit Runge-Kutta schemes and Backward Difference schemes.[6,7,20,39] When dynamic meshes are used, the mesh velocities and other parameters related to the geometry need to be considered carefully so that the errors introduced by the deformation of the mesh do not degrade the formal accuracy of the flow simulation. The discrete geometric conservation law (DGCL) provides a guideline on how to evaluate these quantities. The implementation of high order implicit Runge-Kutta schemes with high order spatial discretization can be very complicated and difficult if the mesh is moving and/or refining and/or coarsening. Space-time methods[3,8,19,21,23,26,35] represent an alternate approach for achieving high-order accuracy in both time and space, simultaneously. Conservative space-time schemes also satisfy the DGCL naturally. Another advantage of space-time schemes is that they provide a framework for maintaining discrete conservation even in the presence of adaptively refining and coarsening meshes.

In this paper, we investigate the combination of space-time schemes and adaptive meshing motion (*r*-refinement) strategies. In the following sections, we first outline the formulation of the governing equations and the base solver. We then discuss our choice of adaptive strategies and implementation of the ghost fluid method within the context of a space-time discretization. Results are then presented to demonstrate the accuracy and effectiveness of the adaptive space-time approach.

II. Base Solver

A general conservation law in three-dimensional space can be written as

$$\frac{\partial \mathbf{u}}{\partial t} + \frac{\partial \mathbf{f_i}}{\partial x_i} = 0 \qquad\qquad i = 1, 2, 3 \tag{1}$$

where $\mathbf{u}$ and $\mathbf{f_i}$ are the vectors of conserved variables and fluxes, respectively. Defining a new flux vector as:

$$\mathbf{F} = (\mathbf{f_1}, \mathbf{f_2}, \mathbf{f_3}, \mathbf{u}) \tag{2}$$

and a new coordinate system as:

$$\bar{\mathbf{x}} = (x_1, x_2, x_3, t) \tag{3}$$

then, equation (1) can be rewritten as

$$\frac{\partial \mathbf{F_i}}{\partial \bar{x}_i} = 0 \qquad\qquad i = 1, 2, 3, 4 \tag{4}$$

The computational domain is divided into non-overlapping elements. The solution in each element can be approximated by a polynomial expansion

$$\mathbf{u}(\bar{\mathbf{x}}) \simeq \sum_{l=1}^{P} \varphi_l(\bar{\mathbf{x}}) \mathbf{u}_l \tag{5}$$

where φ_l represents the $l_t h$ basis function, and $\mathbf{u}_l$ denote the coefficients of the polynomial expansion. In the weak form, equation (4) can be written as

$$\int_\Omega \varphi_j \frac{\partial \mathbf{F_i}}{\partial \bar{x}_i} dV = 0 \tag{6}$$

Integrating by parts, equation (6) becomes

$$\oint_{\partial\Omega} \varphi_j \mathbf{F_i} \bar{n}_i dS - \int_\Omega \frac{\partial \varphi_j}{\partial \bar{x}_i} \mathbf{F_i} dV = 0 \tag{7}$$

In equation (7), the first term corresponds to the surface integration. The flux $\mathbf{F_i}\bar{n}_i$ is replaced by an approximate Riemann flux

$$\mathbf{F_i}\bar{n}_i = \mathbf{H}(\mathbf{u}^-, \mathbf{u}^+, \bar{n}_i) \tag{8}$$

The Riemann flux at the interface used in this paper is set to

$$\mathbf{H}(\mathbf{u}^-, \mathbf{u}^+, \bar{n}_i) = \frac{1}{2}\left(\mathbf{F}_L + \mathbf{F}_R - \left|\frac{\partial \mathbf{F}}{\partial \mathbf{u}}\right|(\mathbf{u}_R - \mathbf{u}_L)\right) \tag{9}$$

Equation (7) becomes

$$\oint_{\partial\Omega} \varphi_j \mathbf{H}(\mathbf{u}^-, \mathbf{u}^+, \bar{n}_i) dS - \int_\Omega \frac{\partial \varphi_j}{\partial \bar{x}_i} \mathbf{F}_\mathbf{i} dV = 0 \tag{10}$$

By using quadrature rules, the two parts in equation (10) can be computed as

$$\oint_{\partial\Omega} \varphi_j \mathbf{H}(\mathbf{u}^-, \mathbf{u}^+, \bar{n}_i) dS = \sum_{\partial\Omega} \sum_k (w_k \mathbf{H}(\mathbf{u}^-, \mathbf{u}^+, \bar{n}_i)|_{\bar{x}_k} \varphi_j(\bar{x}_k))|S| \tag{11}$$

and

$$\int_\Omega \frac{\partial \varphi_j}{\partial \bar{x}_i} \mathbf{F}_\mathbf{i} dV = \sum_k w_k (\frac{\partial \varphi_j}{\partial \bar{x}_i} \mathbf{F}_\mathbf{i})|_{\bar{x}_k} |V| \tag{12}$$

For one-dimensional space time, quadrilateral elements are used, as shown in figure(1). We use Lobatto shape functions as the base functions for the edge, triangle and quadrilateral elements. By defining a residual

$$\mathbf{R} \equiv \oint_{\partial\Omega} \varphi_j \mathbf{H}(\mathbf{u}^-, \mathbf{u}^+, \bar{n}_i) dS - \int_\Omega \frac{\partial \varphi_j}{\partial \bar{x}_i} \mathbf{F}_\mathbf{i} dV \tag{13}$$

the system can be solved by a Newton method as:

$$\left[\frac{\partial \mathbf{R}}{\partial \mathbf{u}}\right] \mathbf{\Delta u} = -\mathbf{R} \tag{14}$$

$$\mathbf{u}^{n+1} = \mathbf{u}^n + \mathbf{\Delta u} \tag{15}$$

where $\left[\frac{\partial \mathbf{R}}{\partial \mathbf{u}}\right]$ denotes the Jacobian of the space-time system.

III. Adaptive Strategies

The objective of adaptive strategies is to achieve increased computational efficiency, or in other words: to obtain the maximum error reduction per unit cost.[18] There are three types of adaptive strategies:

1. r-refinement involves moving the mesh points and adjusting the element sizes to obtain better resolution, as shown in figure(2b). The advantage of r-refinement is the low computational expense of these methods. The drawback of r-refinement is that the accuracy can not be improved beyond a certain level.[17]

2. h-refinement involves increasing/decreasing the number of elements, or refining/coarsening the mesh, as shown in figure(2c). Isotropic h-refinement is the most easily implemented technique, although this approach can result in excessively fine meshes near anisotropic flow features, such as near discontinuities (shocks) or boundary layers.

3. p-refinement involves increasing/decreasing the order of the polynomial, as shown in figure(2d). The performance of p-refinement is better in smooth regions but degrades in non-smooth regions.

By investigating mesh refinement for a strong shock over a cylinder, Yamaleev and Carpenter[38] showed that a sharper shock could be obtained by adding the grid points in the vicinity of the shock, but solution accuracy quantities such as the pressure integral, which may be of greater concern, may not be improved compared to the solution on a uniform grid. It is well known that the discontinuous Galerkin method or discontinuous spectral element method can resolve shocks exactly without suffering from the Gibbs phenomenon if the discontinuity is located exactly on the interface between two elements.[4,16,24,34,38] Many researchers have shown that a sharp discontinuous front can be maintained if the mesh is moved with the front.[31,32] If a discontinuity is detected and grid points can be moved to the position of discontinuity in the computational domain, the discontinuity will only exist at the element interfaces, which will avoid excessively fine mesh adaptation near the shock. Another advantage is that the flow solution is smooth inside

each element, where a high-order p-refinement scheme can perform well and no numerical oscillations will be produced. hp-refinement can be easily applied to these "smooth" solutions according to the theory of maximum reduction in the error per unit cost.[18] In this paper, our focus will be how to track the discontinuity and move the mesh to the discontinuity, and techniques for coupling the tracking technique/r-refinement with a high-order space-time scheme, which has the advantage of handling the mesh moving/adaptation in a natural manner. One of the principal challenges is how to accurately locate the position of discontinuities present in the computation. In the next section, the level set method and Ghost Fluid Method(GFM) will be introduced and their coupling with the proposed space-time scheme will be illustrated.

IV. Shock Front Tracking

According to Touil,[33] an accurate determination of the shock location is difficult to obtain by shock capturing or shock-detection, but can be obtained by a shock-tracking with a level set method. The level set method[25] has the capability of handling complicated topological changes due to the evolution of curves and surfaces. Fedikw[11,12]presented the Ghost Fluid Method to track discontinuities. Aslam[1,2] presented a level set algorithm for discontinuity tracking in hyperbolic conservation laws. Glimm et al also presented a 2nd order conservative front-tracking method[13,14] in the space-time frame. Touil et al.[33] presented a discontinuity tracking method with spectral accuracy. Their idea is to subdivide an element containing a discontinuity into 2^p subcells and each subcell is solved by a first-order accurate scheme, while other elements with "smooth" solution are solved by pth-order polynomials.

The core idea of the level set method for tracking discontinuities presented by Aslam is to avoid discretizing across the discontinuity, which is analogous to the ENO schemes presented by Shu and Osher. Instead of choosing the right interpolation polynomial from many possible candidates(ENO), Aslam defined two functions $u^{(1)}$ and $u^{(2)}$, which are continuous cross the discontinuity. A level set function ψ, which is also a continuous function, is used to locate the position of the discontinuity. There are two states($u^{(1)}$ and $u^{(2)}$) at each mesh point, as shown in figure (3)a. The real solution function u will be $u^{(1)}$ or $u^{(2)}$ depending on the sign of the level set function ψ:

$$u = \begin{cases} u^{(1)} & \text{if } \psi > 0 \\ u^{(2)} & \text{if } \psi \leq 0 \end{cases} \qquad \text{and} \qquad u_g = \begin{cases} u^{(2)} & \text{if } \psi > 0 \\ u^{(1)} & \text{if } \psi \leq 0 \end{cases} \tag{16}$$

where u_g is the ghost state and the discontinuity is located at $\psi = 0$. Even if the function u is discontinuous, the functions $u^{(1)}$, $u^{(2)}$ and ψ are continuous. The algorithm does not deal with the discontinuous function u directly, but instead works on the continuous functions $u^{(1)}$, $u^{(2)}$ and ψ. High-order schemes can be used to discretize these continuous functions. Additional details, such as the precise definition of the ghost states u_g can be found in references[1,2,11,12] Equation (1) can be rewritten as

$$\frac{\partial \mathbf{u^{(1)}}}{\partial t} + \frac{\partial \mathbf{f_i^{(1)}}}{\partial x_i} = 0, \mathbf{u} = \mathbf{u^{(1)}}, \text{if } \psi > 0 \qquad \frac{\partial \mathbf{u^{(2)}}}{\partial t} + \frac{\partial \mathbf{f_i^{(2)}}}{\partial x_i} = 0, \mathbf{u} = \mathbf{u^{(2)}}, \text{if } \psi \leq 0 \tag{17}$$

and the level set equation, which must also be solved, is given by

$$\frac{\partial \psi}{\partial t} + \mathbf{s}_i \frac{\partial \psi}{\partial x_i} = 0 \tag{18}$$

where $\mathbf{s}_i$ is the discontinuity speed and is computed from the two states, $u^{(1)}$ and $u^{(2)}$, by solving the Riemann problem. For a scalar problem, the discontinuity speed is given by

$$s = \frac{f(u_r) - f(u_l)}{u_r - u_l} \tag{19}$$

where $f(u_l)$, $f(u_r)$, u_l and u_r are the left and right flux and state, respectively.

In this paper, the level-set method for tracking discontinuities described by Aslam[1,2] (similar to the ghost-fluid method) is coupled with a space-time Discontinuous Galerkin discretization. The discontinuity is tracked and then fitted by r-refinement in the space-time frame. Cells in the neighborhood of a discontinuity are defined as "troubled cells", as shown in figure (3)b. In these "troubled cells", two states($u^{(1)}$ and $u^{(2)}$) are defined, and two sets of equation (17) are solved. In other cells, only one set of equations (1) is solved. Because the "troubled cells" represent a narrow band along the discontinuity, the overhead introduced by

the "troubled cells" is minimal. All these equations are solved by the high-order space-time Discontinuous Galerkin scheme, after which the speed of the discontinuity $\mathbf{s}_i$, defined by the two states in the "troubled cells", will be computed by solving the Riemann problem or by equation (19).

The level set function $\psi(t^n, x)$ is initialized as the minimum perpendicular distance to the initial location of the discontinuities with $\psi(t^n, x = x_d) = 0$, where x_d is the discontinuity location. The level set equation (18) can be solved to obtain the distribution of $\psi(t, x)$, where $t^n \leq t \leq t^{n+1}$. and $\psi(t, x) = 0$ is the discontinuity position. To improve the accuracy of the discontinuity front location, an iterative approach is introduced, as shown in figure (4)a. Noting that the front speed $v_f^{(1)}$ should be equal to the front speed $v_f^{(2)}$, which is determined by the states on the two sides of the front, the following equation

$$v_f^{(1)}(\psi_t, \psi_x) = v_f^{(2)}(u^-, u^+) \tag{20}$$

must be satisfied. This can be done by solving another level set equation. After the front is located, the mesh points are moved to the front, as shown in figure (4)b. Equation (17) will be rerun and the front/mesh will be adjusted according to equation (20). It should be noted that the front could be a curve in one-dimensional space-time, a curved surface in two-dimensional space-time and a curved hyper-surface in three-dimensional space-time. Therefore, a curved space-time element could be used for improved accuracy, although this has not been attempted in this work.

Compared to the method used by Touil et al.,[33] our method does not need to subdivide the "troubled cells" to subcells, and the time step is not limited by the tiny subcells. Additionally, the front is also tracked in space-time in the current approach. Sollie et al[30] have also developed a space-time Discontinuous Galerkin Method using a level-set method for front tracking. However, their approach makes use of artificial dissipation for capturing the discontinuity, and creates subdivided cells along the discontinuous front. In the current approach, the shock is essentially fit using the mesh motion r-refinement technique and no explicit artificial damping or cell subdivisions are employed.

V. Results and Discussion

To demonstrate the accuracy of the space-time method, the following one-dimensional scalar equation is solved by the current method

$$\frac{\partial u}{\partial t} + a\frac{\partial u}{\partial x} = 0 \tag{21}$$

where a is the wave speed and is set to 1 in this computation. The initial condition is a sine wave given as:

$$u(x, 0) = sin(\pi x) \qquad -1 \leq x \leq 1 \tag{22}$$

A periodic boundary condition is applied on both sides of the domain. The time step is set to $\Delta t = 0.05$ and the total integration time is $T = 6$, which corresponds to 120 time steps. The final solution u is compared with the exact solution u_{exact} which also corresponds to the initial condition. The L_2 error of the solution is monitored, which is defined as:

$$E_{L_2} = \frac{1}{b-a}\int_a^b (u - u_{exact})^2 dx \tag{23}$$

Figure(5a) and (5b) show the solution of the scalar equation. Figure(5c) shows the error versus the number of degrees of freedom for different discretization orders p, where the schemes are seen to be superconvergent. The $p = 1$ scheme achieves an accuracy order of about 4 in the beginning, although this is reduced for larger numbers of degrees of freedom because the temporal error becomes dominant. (Please be noted that the time step is same for all orders.) On the other hand, the $p = 2$, $p = 3$ and $p = 4$ schemes achieve accuracy orders of 6, 8 and 10, respectively.

The second case is a scalar wave (c.f. equation (21)) with a square function prescribed as initial condition. Because of the discontinuous nature of the wave profile, numerical oscillations occur when using a fixed mesh configuration, as shown in figure(6). To eliminate the numerical oscillations, the r-refinement technique is invoked and the results are shown in figure (7). The space-time mesh becomes aligned with the wave propagation direction, and the sharp discontinuity is accurately resolved with no numerical oscillations.

The next case consists of a non-linear problem given by inviscid Burger's equation:

$$\frac{\partial u}{\partial t} + u\frac{\partial u}{\partial x} = 0 \tag{24}$$

with initial condition:

$$u(x,0) = \begin{cases} 1 & \text{if } -2.5 \leq x < -1 \\ 1 + \frac{1}{8}(1 + cos(\pi x)) & \text{if } -1 \leq x \leq 0 \\ 1 - \frac{1}{8}(1 + cos(\pi x)) & \text{if } 0 < x \leq 1 \\ 1 & \text{if } 1 < x \leq 7.5 \end{cases} \tag{25}$$

The boundary condition is set to be periodic in space. Burger's equation with this initial condition has a sharp front at $x = 0$, which propagates to the right with a steepening profile. This case was used by Touil et al.[33] to test the accuracy of their method. In this case, the front speed is not set explicitly as previously, but is now part of the solution. Equations (17) are solved in the "troubled cells" to get two states $u^{(1)}$ and $u^{(2)}$. The velocity at each mesh point is computed by equation (19). Then, the level-set equation (18) is solved to determine the front position ($\psi = 0$) and equation (20) must be satisfied by moving the front position. The mesh is then moved to the front position and equations (17) are solved again. Figure (8) shows the solution from $t = 0$ to $t = 6$ for $p = 3$. The time step is 0.1 and 100 elements are used. A sharp front is maintained at all times, and no oscillations are present. Figure (9)a shows the convergence of the shock position. The error in the shock position for high p-order ($p = 4$ and $p = 5$) does not decrease due to the error torrance for the iteration of equation (20) which is set to 10^{-13}. Figure (9)b shows the L_2 error of the solution versus different discretization orders p. The definition of the L_2 error is given by equation (23) and the integration is done by Gauss numerical integration. As the discretization order p increases, the error is seen to decrease rapidly. Figure (9)c shows the error versus the number of degrees of freedom for different discretization orders p. The design accuracy is achieved. The $p = 1$ scheme achieves an accuracy order of about 2.01, and the $p = 2$ and $p = 3$ schemes achieve accuracy orders of 2.89 and 3.88, respectively.

VI. Conclusion

A high-order space-time scheme has been coupled with a level-set discontinuity tracking method. The mesh is adaptively moved with the discontinuity which is tracked by the level set method. An iteration method is employed to improve the accuracy of the computed shock position. Numerical results in one spatial dimension illustrate the ability to capture and maintain sharp discontinuous profiles without any additional artificial damping. The high-order space-time scheme delivers design accuracy even in the presence of discontinuities. Future work will concentrate on extensions to higher spatial dimensions, as well as the introduction of more accurate space-time curved elements.

VII. Acknowledgments

This work was partly funded under NASA Grant NNX07AC31A.

References

[1]T. D. Aslam. A level-set algorithm for tracking discontinuities in hyperbolic conservation laws, I. scalar equations. *Journal of Computational Physics*, 167:413–438, 2001.

[2]T. D. Aslam. A level-set algorithm for tracking discontinuities in hyperbolic conservation laws, II. systems of equations. *Journal of Computational Physics*, 19:37–62, 2003.

[3]P. Bar-Yoseph. Space-time discontinuous finite element approximations for multi-dimensional nonlinear hyperbolic systems. *Computational Mechanics*, 5:145–160, 1989.

[4]P. Bar-Yoseph and D. Elata. An efficient L2 galerkin finite element method for multi-dimensional non-linear hyperbolic systems. *International Journal for Numerical Methods in Engineering*, 29:1229–1245, 1990.

[5]F. Bassi and S. Rebay. High-order accurate discontinuous finite element solution of the 2D euler equations. *Journal of Computational Physics*, 138:251–285, 1997.

[6]H. Bijl, M. H. Carpenter, V. N. Vatsa, and C. A. Kennedy. Implicit time integration schemes for the unsteady incompressible Navier-Stokes equations: laminar flow. *Journal of Computational Physics*, 179(1):313–329, 2002.

[7]J. Butcher. Implicit runge-kutta processes. *Mathematics of Computation*, 18:50–64, 1964.

[8]J. Chessa and T. Belytschko. Arbitrary discontinuities in space-time finite elements by level sets and X-FEM. *International Journal for Numerical Methods in Engineering*, 61:2595–2614, 2004.

[9]B. Cockburn and C. W. Shu. TVB Runge-Kutta local projection discountinuous Galerkin finite element method for conservation laws II: general framework. *Mathematics of Computation*, 52:411–435, 1989.

[10]L. Demkowicz, W. Rachowicz, and P. Devloo. A fully automatic hp-adaptivity. *Journal of Scientific Computing*, 17:117–142, 2002.

[11]R. P. Fedkiw, T. Aslam, B. Merriman, and S. Osher. A non-oscillatory eulerian approach to interfaces in multimaterial flows (the ghost fluid method). *Journal of Computational Physics*, 152:457–492, 1999.

[12]R. P. Fedkiw, T. Aslam, and S. Xu. The ghost fluid method for deflagration and detonation discontinuities. *Journal of Computational Physics*, 154:393–427, 1999.

[13]J. Glimm, X. Li, Y. Liu, Z. Xu, and N. Zhao. Conservative front tracking with improved accuracy. *SIAM Journal on Numerical Analysis*, 41:1926–1947, 2003.

[14]J. Glimm, X. Li, Y. Liu, and N. Zhao. Conservative from tracking and level set algorithms. volume 98, pages 14198–14201, 2001.

[15]W. Gui and I. Babuska. The h, p and h-p versions of the finite element method in 1 dimension. part III: The adaptive h-p version. *Numerische Mathematik*, 49:659–683, 1986.

[16]A. Harten and J. M. Hyman. Self-adjusting grid methods for one-dimensional hyperbolic conservation laws. *Journal of Computational Physics*, 50:235–269, 1983.

[17]D. F. Hawken, J. J. Gottlieb, and J. S. Hansen. Review of some adaptive node-movement techniques in finite element and finite difference solutions of partial differential equations. *Journal of Computational Physics*, 95:254–302, 1991.

[18]P. Houston and E. Suli. A note on the design of hp-adaptive finite element methods for elliptic partial differential equations. *Computer Methods in Applied Mechanics and Engineering*, 194:229–243, 2005.

[19]P. G. Huang, Z. J. Wang, and Y. Liu. An implicit space-time spectral difference method for discontinuity capturing using adaptive polynomials. AIAA 2005-5255, 2005.

[20]G. Jothiprasad, D. J. Mavriplis, and D. A. Caughey. Higher-order time integration schemes for the unsteady navier stokes equations on unstructured meshes. *Journal of Computational Physics*, 191:542–566, 2003.

[21]C. M. Klaij, J. van der Vegt, and H. van der Ven. Space-time discontinuous galerkin method for the compressible navier-stokes equations. *Journal of Computational Physics*, 217:589–611, 2006.

[22]Y. Liu, M. Vinokur, and Z. J. Wang. Discontinuous spectral difference method for conservation laws on unstructured grids. Proceedings of the 3rd International Conference in CFD, 2004.

[23]R. Lowrie. *Compact Higher-Order Numerical Methods for Hyperbolic Conservation Laws*. PhD thesis, University of Michigan, 1996. http://www.engin.umich.edu/research/cfd/research-publications.

[24]C. Mavriplis. Adaptive mesh strategies for the spectral element method. *Computer Methods in Applied Mechanics and Engineering*, 116:77–86, 1994.

[25]S. Osher and J. A. Sethian. Fronts propagating with curvature-dependent speed: algorithms based on hamilton-jacobi formulations. *Journal of Computational Physics*, 79:12–49, 1988.

[26]J. Palaniappan, R. B. Haber, and R. L. Jerrard. A spacetime discontinuous galerkin method for scalar conservation laws. *Computer Methods in Applied Mechanics and Engineering*, 193:3607–3631, 2004.

[27]P.-O. Persson and J. Peraire. Sub-cell shock capturing for discontinuous galerkin methods. AIAA 2006-112, 2006.

[28]J. Qiu and C. W. Shu. A comparison of trouble cell indicators for runge-kutta discontinuous galerkin method using weno limiters. *SIAM Journal on Scientific Computing*, 27:995–1013, 2005.

[29]W. Rachowicz, J. T. Oden, and L. Demkowicz. Toward a universal h-p adaptive finite element strategy part 3. design of h-p meshes. *Computer Methods in Applied Mechanics and Engineering*, 77:181–212, 1989.

[30]W. E. H. Sollie, J. J. W. van der Vegt, and O. Bokhove. A space-time discontinuous galerkin finite element method for two-fluid problems. Memorandum 1849 (August 2007). http://www.math.utwente.nl/publications, 2007.

[31]T. Tezduyar, M. Behr, and J. Liou. A new strategy for finite element computations involving moving boundaries and interfaces-the deforming-spatial-domain/space-time procedure: I. the concept and the preliminary numerical tests. *Computer Methods in Applied Mechanics and Engineering*, 94:339–351, 1992.

[32]T. Tezduyar, M. Behr, S. Mittal, and J. Liou. A new strategy for finite element computations involving moving boundaries and interfaces - the deforming-spatial-domain/space-time procedure: Ii. computation of free-surface flows, two-liquid flows, and flows with drifting cylinders. *Computer Methods in Applied Mechanics and Engineering*, 94:353–371, 1992.

[33]H. Touil, M. Y. Hussaini, and M. Sussman. Tracking discontinuities in hyperbolic conservation laws with spectral accuracy. *Journal of Computational Physics*, 225:1810–1826, 2007.

[34]J. Y. Trepanier, M. Paraschivoiu, M. Reggio, and R. Camarero. A conservative shock fitting method on unstructured grids. *Journal of Computational Physics*, 126:421–433, 1996.

[35]H. van der Ven and J. van der Vegt. Space-time discontinuous galerkin finite element method with dynamic grid motion for inviscid compressible flows: Ii. efficient flux quadrature. *Computer Methods in Applied Mechanics and Engineering*, 191:4747–4780, 2002.

[36]Z. J. Wang. Spectral (finite) volume method for conservation laws on unstructured grids: I. basic formulation. *Journal of Computational Physics*, 178:210, 2002.

[37]Z. J. Wang and Y. Liu. Spectral (finite) volume method for conservation laws on unstructured grids: II. extension to two- dimensional scalar equation. *Journal of Computational Physics*, 179:665–697, 2002.

[38]N. K. Yamaleev and M. H. Carpenter. On accuracy of adaptive grid methods for captured shocks. *Journal of Computational Physics*, 181:280–316, 2002.

[39]Z. Yang and D. J. Mavriplis. Higher-order time integration schemes for aeroelastic applications on unstructured meshes. AIAA Paper 2006-441, also published in AIAA Journal, 2006.

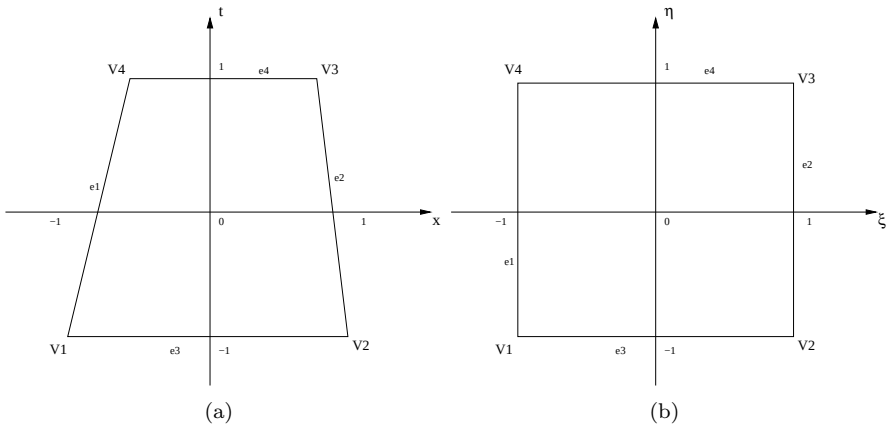

Figure 1. Illustration of space-time elements in (a) physical space (b) isoparametric space

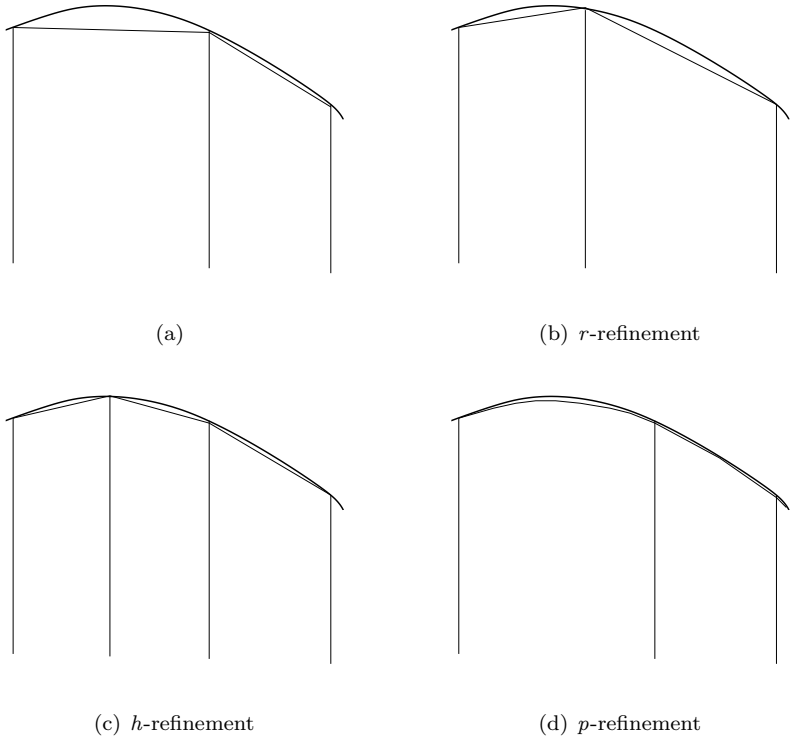

Figure 2. One-dimensional illustration of various potential adaptive-meshing strategies.

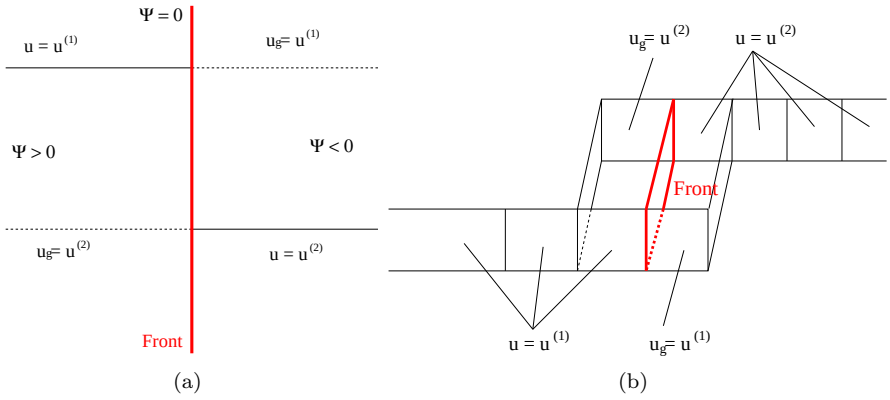

Figure 3. Illustration of the two states for the Ghost Fluid Method.

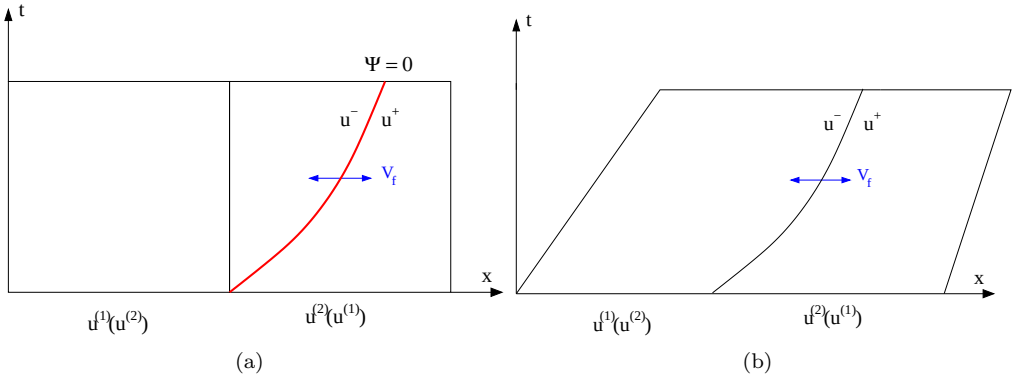

Figure 4. Illustration of front tracking in space-time.

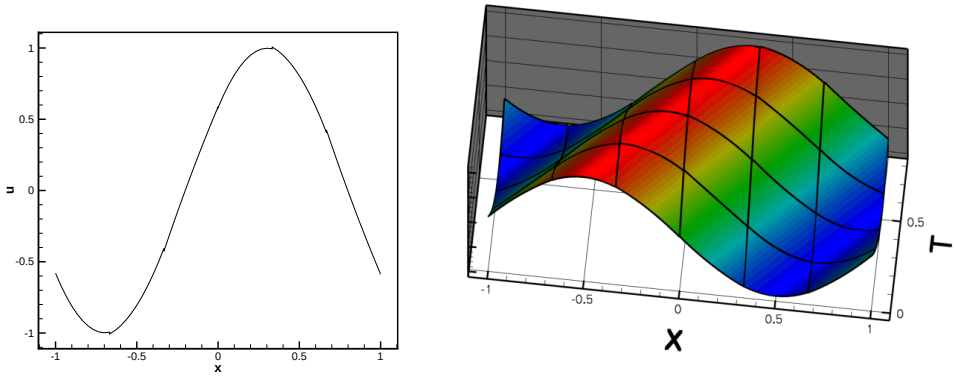

(a) (b)

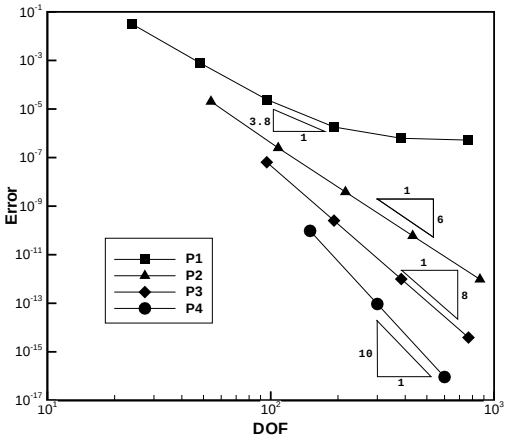

(c)

Figure 5. Numerical solution of the moving sine wave problem at (a) final time, (b) in space-time, and (c) accuracy comparison for different orders of accuracy p.

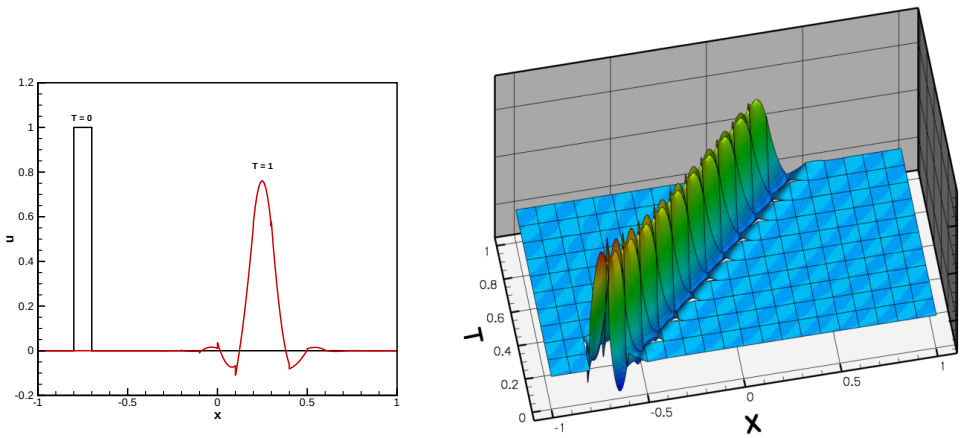

(a) (b)

Figure 6. Moving square-wave solution resolved using p=2 on a fixed mesh

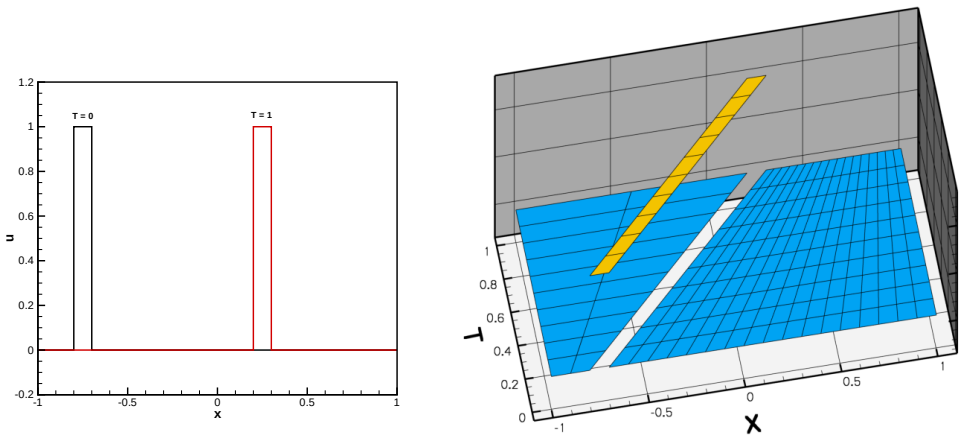

(a) (b)

Figure 7. Moving square-wave solution resolved using adaptively moving mesh/r-refinement, p = 2.

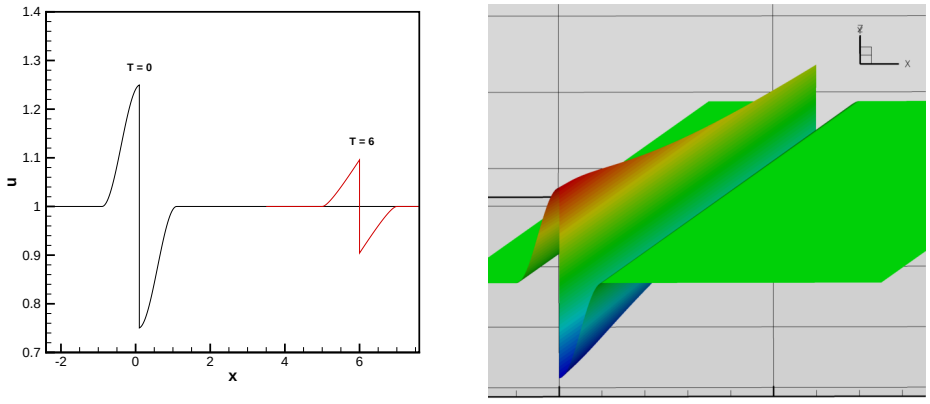

(a) (b)

Figure 8. The solution of inviscid Burger's equation on adaptively moving mesh with p = 3.

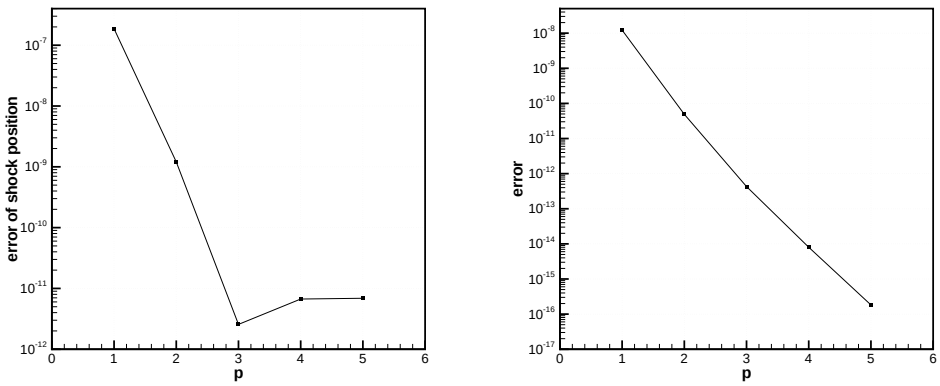

(a) (b)

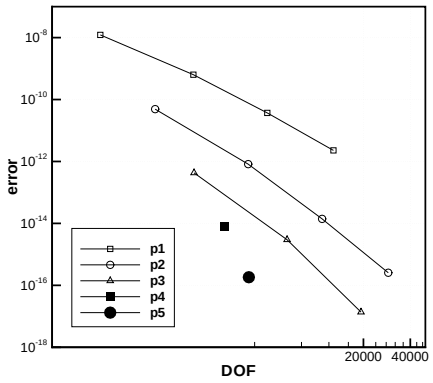

(c)

Figure 9. Computed error for inviscid Burger's equation problem. (a) Error in shock position versus order of discretization p. (b) Error in final solution versus discretization order p. (c) Error in final solution versus number of degrees of freedom.